

## RESEARCH ARTICLE

# Dislocation toughening in single-crystal KNbO<sub>3</sub>

Oliver Preuß<sup>1</sup> | Enrico Bruder<sup>2</sup> | Wenjun Lu<sup>3</sup> | Fangping Zhuo<sup>1</sup>  |  
Christian Minnert<sup>2</sup> | Jiawen Zhang<sup>3</sup> | Jürgen Rödel<sup>1</sup> | Xufei Fang<sup>1</sup> 

<sup>1</sup>Division Nonmetallic-Inorganic Materials, Department of Materials and Earth Sciences, Technical University of Darmstadt, Darmstadt, Germany

<sup>2</sup>Division Physical Metallurgy, Department of Materials and Earth Sciences, Technical University of Darmstadt, Darmstadt, Germany

<sup>3</sup>Department of Mechanical and Energy Engineering, Southern University of Science and Technology, Shenzhen, P. R. China

**Correspondence**

Oliver Preuß and Xufei Fang, Division Nonmetallic-Inorganic Materials, Department of Materials and Earth Sciences, Technical University of Darmstadt, Alarich-Weiss Str. 2, 64287 Darmstadt, Germany.  
Email: [preuss@ceramics.tu-darmstadt.de](mailto:preuss@ceramics.tu-darmstadt.de) and [fang@ceramics.tu-darmstadt.de](mailto:fang@ceramics.tu-darmstadt.de)

**Funding information**

DFG, Grant/Award Number: 414179371

**Editor's Choice**

The Editor-in-Chief recommends this outstanding article.

**Abstract**

The growing research interest in dislocation-tuned functionality in ceramics is evident, with the most recent proofs-of-concept for enhanced ferroelectric properties, electrical conductivity, and superconductivity via dislocations. In this work, we focus on dislocation-tuned mechanical properties and demonstrate that, by engineering high dislocation densities (up to  $10^{14} \text{ m}^{-2}$ ) into KNbO<sub>3</sub> at room temperature, the fracture toughness can be improved by a factor of 2.8. The microstructures, including dislocations and domain walls, are examined by optical microscopy, electron channeling contrast imaging, piezo-response force microscopy, and transmission electron microscopy methods to shed light on the toughening mechanisms. In addition, high-temperature (above the Curie temperature of KNbO<sub>3</sub>) indentation tests were performed to exclude the influence of ferroelastic toughening, such that the origin of the toughening effect is pinpointed to be dislocations.

**KEYWORDS**

dislocation, dislocation toughening, fracture toughness, oxide perovskite, room-temperature plasticity

## 1 | INTRODUCTION

The brittleness of ceramics has long been considered a major drawback for taking advantage of their otherwise superb mechanical properties like high stiffness, strength, low fatigue susceptibility, high-temperature stability, and overall chemical inertness.<sup>1</sup> This brittleness of ceramics stems from: (a) The type of atomic bonds, which are ionic and/or covalent in character, and (b) the sensitivity to flaws

and cracks, which inevitably come along with processing and machining processes.

For the past decades, various toughening mechanisms have been developed for ceramics, such as crack bridging, process zone toughening, and crack deflection.<sup>2</sup> Still, the fracture toughness of ceramics (typically  $1\text{--}10 \text{ MPa m}^{0.5}$ ) is lacking behind that of typical engineering metals like steel, aluminum, and copper alloys (typically  $30\text{--}150 \text{ MPa m}^{0.5}$ ) by 1–2 orders of magnitude.<sup>3</sup> Toughening in metals is

This is an open access article under the terms of the [Creative Commons Attribution](https://creativecommons.org/licenses/by/4.0/) License, which permits use, distribution and reproduction in any medium, provided the original work is properly cited.

© 2023 The Authors. *Journal of the American Ceramic Society* published by Wiley Periodicals LLC on behalf of American Ceramic Society.

predominantly governed by dislocation activities, which are strongly impeded in ceramics due to the lack of dislocation mobility and multiplication, particularly at room temperature. The pertinent question then arises, provided that dislocations can be engineered into ceramics, could they be utilized for increasing the fracture toughness in ceramics?

Dislocations in ceramics have been investigated since the 1950s, most prominently by Gilman and Johnston in LiF.<sup>4–8</sup> An overview of the current understanding of the general dislocation mechanics in ceramics has been provided by Porz recently.<sup>9</sup> The understanding of dislocation nucleation, multiplication, and motion proposed by Gilman and Johnston can be borrowed to lay the foundation for the dislocation mechanics in ceramics. On the other hand, recently the dislocation-mediated functional properties in ceramics have attracted increasing research interest, be it superconductivity,<sup>10</sup> electrical conductivity,<sup>11</sup> or ferroelectric properties.<sup>12</sup> These discoveries inaugurate a new dimension of engineering functional ceramics. Especially the high-temperature stability of dislocations gives an advantage over “traditional” point defect engineering.<sup>13</sup> Before these properties can be used reliably on a larger scale, the mechanical behavior, which is strongly influenced by the presence of dislocations, needs to be optimized to avoid cracking, and thus, failure of a possible future device based on dislocations.

Previous studies on dislocations in ceramics, although very limited, suggest that dislocations themselves can already enhance the mechanical robustness through dislocation-based enhancement of fracture toughness. Appel et al. observed a plastic zone in front of a crack tip in MgO similar to metals using in situ high voltage electron microscopy in 1979.<sup>14</sup> Narita et al. revealed the toughening effect of dislocations in NaCl single crystals as early as 1985 by cracking notched cantilevers at 77 K with and without an annealing step beforehand.<sup>15</sup> In 1989, Narita et al. came up with the shielding effect of dislocations emitted by the crack tip, lowering the stress intensity factor.<sup>16</sup> A toughening effect by dislocations with annealing of yttrium aluminum garnet at 1500°C for 24 h was achieved by Moon and Saka in 2000.<sup>17</sup> Most recently, Porz et al. achieved a doubling of the crack tip toughness by introducing a high surface dislocation density of  $\sim 10^{15} \text{ m}^{-2}$  into single-crystal SrTiO<sub>3</sub>.<sup>18</sup> Issa et al. demonstrated the size effect in the induced brittle to ductile transition of silicon and the resulting toughening effect.<sup>19</sup> Furthermore, Salem et al. have reported a  $\sim 20\%$  increase of fracture toughness in SrTiO<sub>3</sub> by introducing a high dislocation density via cyclic Brinell ball indentation and subsequent annealing of the crystals at 1100°C.<sup>20</sup>

One of the requirements for effective dislocation toughening, as well as crystal plasticity in general, is a high density of dislocations that are mobile.<sup>18</sup> In the case

of metals, the crack tip itself emits dislocations, which is scarcely observed in ceramics at room temperature. In the works presented above, the dislocation density was either naturally generated by the crack tip, which turns out to be extremely difficult, or, as in the case of Porz et al.,<sup>18</sup> pre-engineered artificially through surface polishing. Additionally, in the case of polycrystals, five independent slip systems are required to fulfill the Taylor criterion<sup>21</sup> for arbitrary plastic deformation to avoid dislocation pileup at grain boundaries and causing grain boundary cracking, which is why this work focuses on single crystals.

In this work, a high dislocation density up to  $4 \times 10^{13} \text{ m}^{-2}$  is introduced in an area of  $\sim 100 \mu\text{m}$  in diameter on potassium niobate (KNbO<sub>3</sub>) by cyclic Brinell indentation, based on the experimental approach developed by Okafor et al. on single-crystal SrTiO<sub>3</sub>.<sup>22</sup> KNbO<sub>3</sub> has been found to exhibit plastic deformation very similar to strontium titanate, with even lower yield strength.<sup>23–25</sup> Cracks are then introduced by Vickers indentation inside these plastic zones to quantify the toughening effect as a function of the dislocation density. The influence of the ferroelectric domain structure in KNbO<sub>3</sub> is then excluded by high-temperature indentation tests above the Curie temperature.

## 2 | EXPERIMENTAL PROCEDURES

### 2.1 | Material

Undoped KNbO<sub>3</sub> (KNO) single crystals prepared by top-seeded solution growth were used for the experiment (FEE GmbH, a division of EOT, Idar-Oberstein, Germany). The room-temperature slip systems are  $\langle 110 \rangle \{110\}$ .<sup>24</sup> KNO has an orthorhombic crystal structure at room temperature. It undergoes two phase transitions with rising temperature, namely, from orthorhombic to tetragonal at 225°C, and from tetragonal to cubic at 435°C.<sup>25</sup> The latter is also the Curie temperature, as both orthorhombic and tetragonal KNbO<sub>3</sub> show ferroelectric behavior. The crystallographic directions given here should be understood as pseudo-cubic directions.

The samples were cut to the dimension of 4 mm × 4 mm × 1.5 mm with the (001) surface being tested. After cutting, the samples were hand-ground with P800, P1200, P2500, and P4000 wet grinding paper (QATM, Mammelzen, Germany), each until at least three times the particle size of the grinding paper was removed. Then, the samples were further half-automatically polished (Phoenix 4000, Buehler, Lake Bluff, IL, USA) with 6, 3, 1, and 1/4 μm diamond polishing paste for 30 min each. The final polishing was done with vibrational polishing

using polishing solution containing ~50 nm colloidal silica particles (OP-S) for 20 h. The final sample thickness was ~1 mm.

## 2.2 | Dislocation generation

To introduce a high dislocation density into KNO, we used the cyclic Brinell indentation method.<sup>22</sup> The tests were performed on a universal indenter machine (Finotest, Karl Frank GmbH, Weinheim-Birkenau, Germany) with a Brinell indenter tip diameter of 2.5 mm and a load of 14.72 N (1.5 kgf). The zones created have a diameter of about 150  $\mu\text{m}$  and a depth of about 400–500 nm measured by a 3D stereo laser microscope (LEXT OLS4000, Olympus IMS, Waltham, USA, see Figure S1 in the supplementary materials). The loading procedure did not leave any visible cracks by optical microscopy in KNO up to cycle counts of 50 $\times$  (“ $\times$ ” means cycle). For this work, Brinell cycle counts of 1 $\times$ , 10 $\times$ , and 25 $\times$  were used to obtain a range of dislocation densities in KNO as will be presented later. For reproducibility and statistical analysis, five Brinell plastic zones were made for each cycle count to ensure a sufficient area for performing multiple Vickers indents inside these Brinell plastic zones.

The successful dislocation generation was verified by inspecting the slip traces by optical microscopy (ZEISS Axio Imager 2, Carl Zeiss Microscopy GmbH, Jena, Germany) with the circular-differential interference contrast (C-DIC) imaging mode. Piezo-response force microscopy (PFM, Cypher atomic force microscope, Asylum Research, Santa Barbara, CA, USA) was utilized to characterize the domain structure. The cantilever was made from conductive Cr-/Pt-coated Si with a nominal free resonance frequency of 75 kHz and a spring constant of 3 N/m.

## 2.3 | Dislocation characterization

The dislocation arrangement and the possible correlation to the domain structure were examined using electron channeling contrast imaging (ECCI)<sup>26</sup> and PFM. Based on these images, the dislocation density can be estimated as a function of cycle count.

To further confirm the dislocations in a 10 $\times$  Brinell zone underneath the surface, a TEM (transmission electron microscope) specimen with a dimension of  $8 \times 2 \times 6 \mu\text{m}^3$  in (100) orientation was prepared from a 10 $\times$  Brinell zone using a dual-beam focused ion beam (FIB)/scanning electron microscope (SEM) instrument (Helios Nanolab 600i, FEI, Hillsboro, USA). Scanning TEM (STEM) imaging was conducted in an aberration-corrected STEM (Titan

Themis, FEI, Hillsboro, USA) at an operating voltage of 300 kV. For annular bright field imaging, a probe semi-convergence angle of 23 mrad and an inner and outer semi-collection angle of 12–22 mrad were implemented.

## 2.4 | Mechanical testing

### 2.4.1 | Room-temperature Vickers indentation

To evaluate the effect of dislocations on the fracture toughness, Vickers indents with an optimized load of 245 mN (25 gf) were induced into the Brinell plastic zones of different cycle counts and, for reference, also into the pristine region. The Vickers indent orientation to the sample (and its cleavage planes) was chosen in a way that four cracks are initiated from the corners (Figure 1A), with sufficient spacing in between to avoid overlapping stress fields. To ensure statistical analysis, a “5  $\times$  5 checkerboard pattern” (Figure 1B) was used, overlaying the entire Brinell zone with Vickers indents. The asymmetry of some crack patterns was addressed by measuring the length of all four emerging cracks individually. As a Palmqvist crack was assumed, the length  $l$  was measured from the “Root” position (where the extrapolated edges of the Vickers indent meet the crack) to the “Tip” position (where the crack ends on the surface), as illustrated in Figure 1A.

The quantification of crack length was performed using an optical microscope (bright field). In total, 52 crack lengths per cycle count (pristine, 1 $\times$ , 10 $\times$ , and 25 $\times$ ) were analyzed.

For further comparison of the fracture toughness between pristine sites and 25 $\times$  Brinell zones (to obtain the maximum effect), the crack tip opening displacement (CTOD) technique was used on the same sample.<sup>27–29</sup> SEM images with a magnification of 50 000 $\times$ , a working distance of 8 mm and an acceleration voltage of 5 kV were made using a Tescan MIRA3-XM (Tescan, Brno, Czech Republic), with a resulting resolution of 4 nm. After the crack tip position was identified, the crack opening was quantified every 0.1  $\mu\text{m}$  for 3  $\mu\text{m}$  from the crack tip. The results were then fitted with the Irwin parabola to obtain the crack tip toughness.<sup>28,30</sup>

Note that the indentation crack length (ICL) method for quantifying fracture toughness has been subject to prolonged discussion.<sup>31</sup> As a Palmqvist crack system is expected for simple radial cracks in plastically deformable ceramics (same in single-crystal SrTiO<sub>3</sub><sup>20</sup>), the Niihara<sup>32</sup> model was adopted to quantify the  $K_{Ic}$  values based on our crack length analysis, with other further ICL methods for comparison.

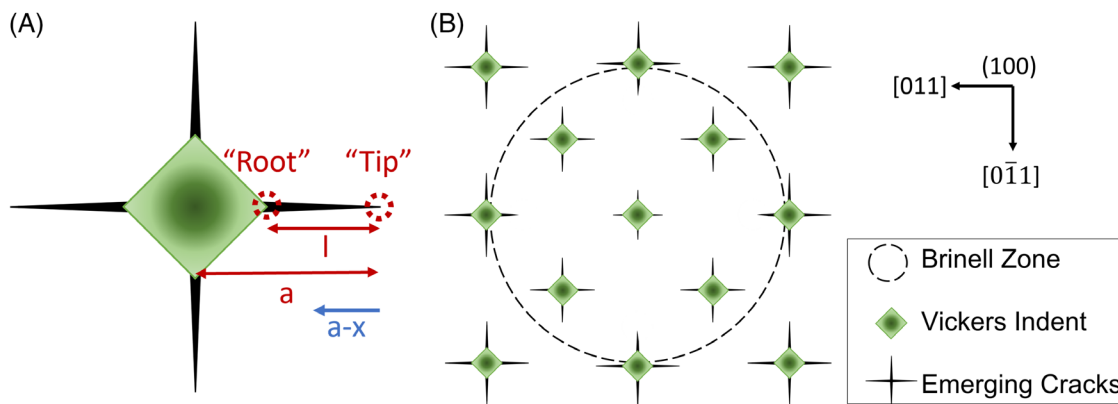


**FIGURE 1** (A) Schematic Vickers indent with cracks emerging from corners, with marked positions for the “Root” and “Tip” of a crack. (B) Schematic Vickers indent pattern relative to the pre-generated Brinell plastic zone. The sample orientation is also indicated.

## 2.4.2 | High-temperature indentation

The possible influence of the ferroelectric domains in the form of ferroelastic toughening was excluded by testing above the Curie temperature (435°C). This technique includes three testing stages. First, at room temperature, the cyclic Brinell indentation was performed to create plastic zones with high dislocation density. The cycle count was 10×, as the dislocation density saturates around this value (Figure 2). Unlike the room-temperature experiments, a 5 mm diameter Ball indenter with a load of 29.4 N (3 kgf) was used to enlarge the plastic zone. The sample’s edges have been chamfered using P4000 wet sandpaper to avoid the growth of big cracks from the edge into the area of interest.

In the second stage, the sample was placed in an ultrahigh-temperature nanoindenter (Nanomechanics/KLA, Milpitas, USA) that is installed horizontally in an SEM chamber (TESCAN VEGA3, Brno, Czech Republic). Heating of the sample to 480°C was done with a rate of 2°C/min to avoid thermal shock. The thermal stability of dislocations up to this temperature has been first confirmed in a pretest through observation of the slip traces using in situ optical microscopy with a heating stage. The surface temperature of the sample was assured by using the indenter as a thermo probe. Indents were then made with a Vickers tip and a load of 250 mN to mimic the mesoscopic tests. Three arrays of 5 × 6 indents were made overlaying the Brinell zones.

In the third stage, we cool down the sample to room temperature with a rate of 1°C/min inside the SEM chamber, the crack patterns were then investigated using an optical microscope to locate the Brinell plastic zones in circumferential differential interference contrast mode and a 3D Stereo LASER Microscope (LEXT OLS4000, Olympus IMS, Waltham, USA) for better topography contrast.

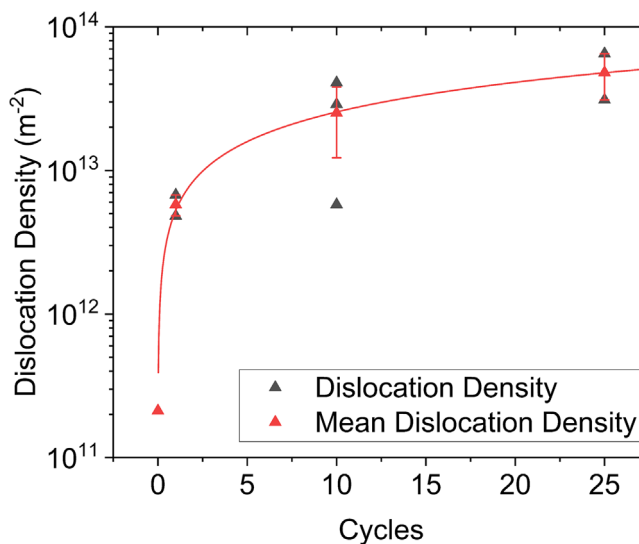


**FIGURE 2** Estimated dislocation density as a function of the cycle count. The dislocation density data was fitted with a linear function (red line).

## 3 | RESULTS AND ANALYSES

### 3.1 | Dislocation characterization

By counting the intersections of dislocation lines with the surface (evidenced by the white dots in ECCI images) in a selected area, the dislocation density for different sites can be estimated. Figure 2 displays the dislocation density calculated as a function of the cycle count of the Brinell zones. The pristine region is characterized by a dislocation density of  $2 \times 10^{11} \text{ m}^{-2}$ . A single cycle of Brinell indentation increases the dislocation density up to  $6 \times 10^{12} \text{ m}^{-2}$  and 25 cycles to  $4 \times 10^{13} \text{ m}^{-2}$ . This marks about a 200-fold increase in dislocation density from pristine to deformed regions using this simple technique.

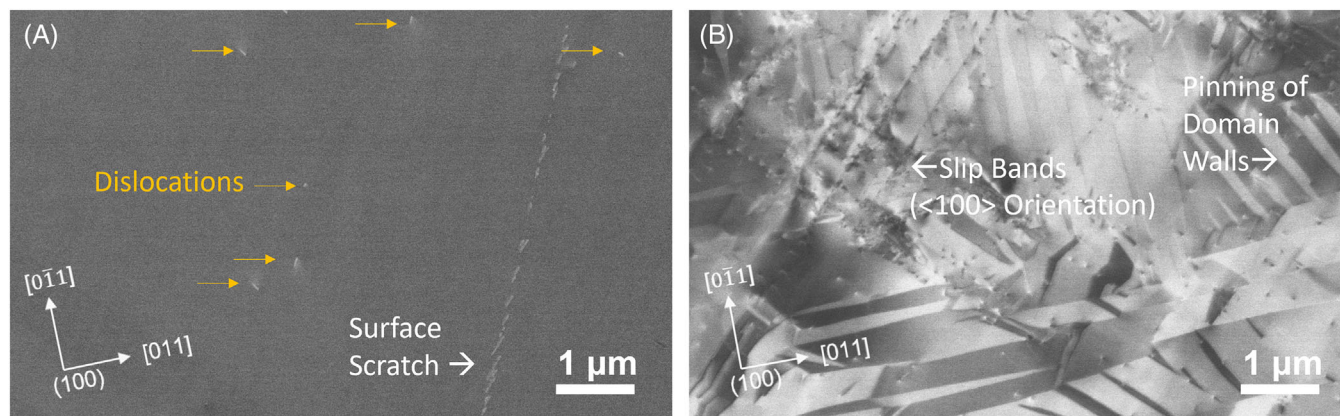


FIGURE 3 Electron channeling contrast imaging (ECCI) images of (A) reference surface and (B) center of 10× Brinell zone.

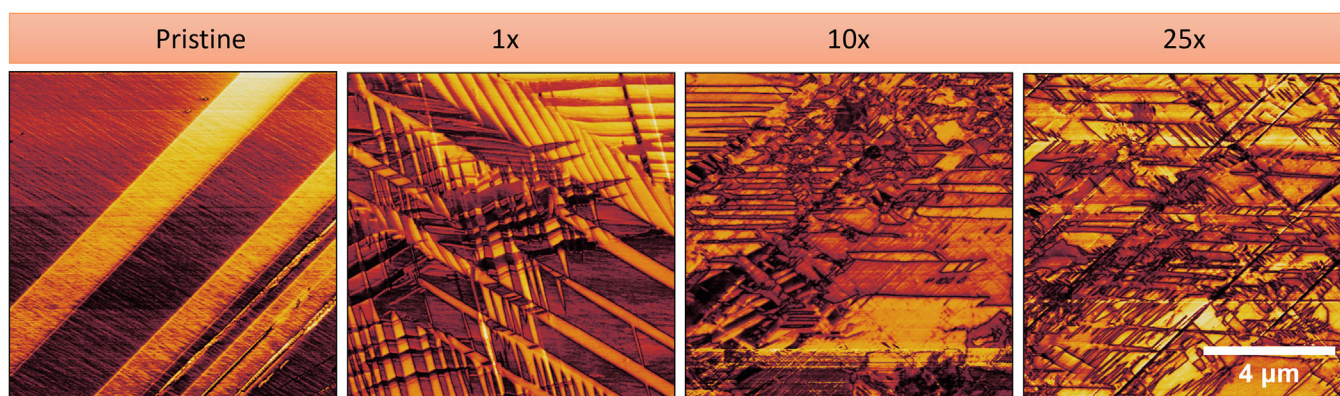


FIGURE 4 Representative piezo-response force microscopy images (phase amplitude) of Brinell zones with different cycle counts.

Figure 3A depicts an ECCI image of the reference surface. Apart from one major surface scratch, only a few single dislocations are visible. The typical stripe pattern from the domain structure (as in Figure 3B) is hardly visible on the reference surface, which is typical for out-of-plane domains under these imaging conditions.

Inside a Brinell zone (Figure 3B), numerous dislocations are visible along the narrow slip bands in  $\langle 100 \rangle$  orientation. Another interesting feature is that some randomly distributed, scattered dislocations are observed to be highly correlated with the domain patterns. For instance, in some cases, the domains have zigzag patterns with dislocations located at the “shoulders” of the domain stripes. This is direct evidence for a strong interaction of dislocations and domain walls (the “pinning effect”), which has been reported before.<sup>12</sup>

In addition, the domain structure is heavily fragmented, with small needle domains extending in various directions. The reason could be that the domain walls are so immobile due to the pinning by the dislocations, that nucleation of new domains is favored over domain wall movement.

The domain fragmentation with increasing cycle count is mostly evident in the PFM images (Figure 4).

Apart from the top-surface characterization, the region several micrometers beneath the surface, as prepared by the TEM specimen (Figure 5A), reveals some dislocations. These dislocations lie in the direction with  $45^\circ$  with respect to the  $\langle 100 \rangle$  direction, which fit to the  $\langle 100 \rangle \{110\}$  slip system typically found in  $\text{KNbO}_3$  deformed at room temperature.<sup>25</sup> The Burgers vector  $[110]$  was verified by the  $\mathbf{g}\cdot\mathbf{b}$  analysis (see Figure S2 in the supplementary materials). It is noted that a region of slightly higher local dislocation density is found around a vertical line feature. This feature is most probably the cross-section of a domain wall. Going up in magnification, Figure 5B highlights a dislocation dipole.

### 3.2 | Crack shortening

The cracks introduced by Vickers indentation inside the Brinell zone (white dashed circle in Figure 6) demonstrate

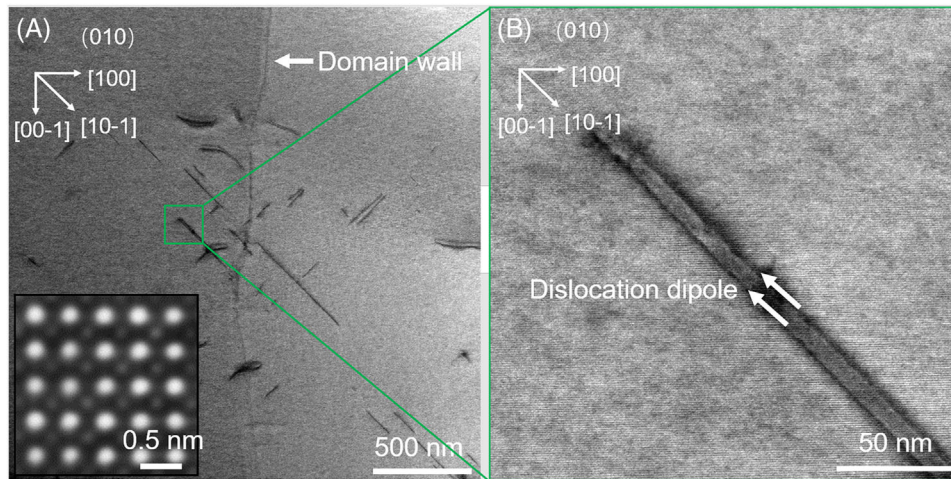


**FIGURE 5** Transmission electron microscopy (TEM) images of focused ion beam (FIB) lamella cut out of a  $10\times$  Brinell zone: (A) dislocations at domain wall, (B) detailed view of dislocation dipole, corresponding to the highlighted region in (A).

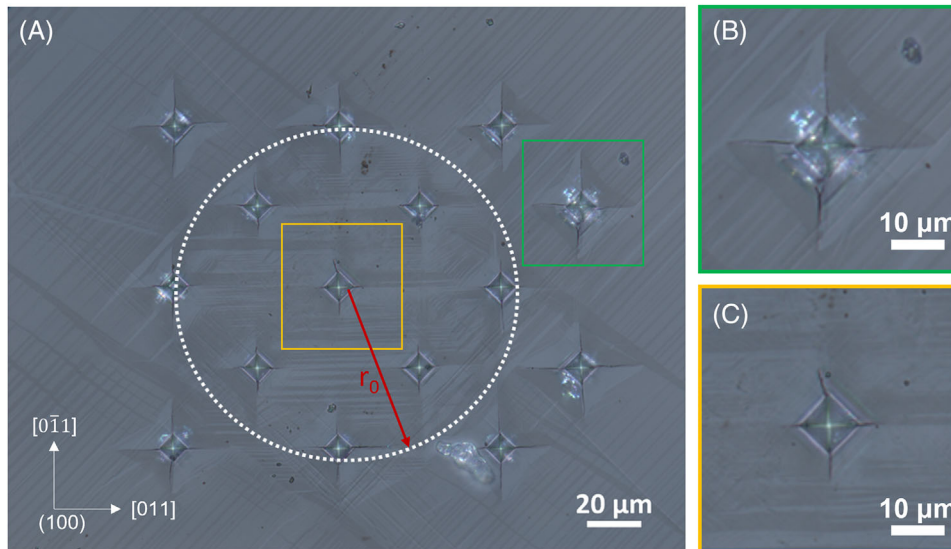


**FIGURE 6** Polarized light microscopy image of crack shortening effect in  $\text{KNbO}_3$ , where the white dotted circle indicates the Brinell plastic zone: (A) entire Brinell zone overlaid with Vickers indents; (B) detailed view of 245 mN (25 gf) Vickers indent and crack system on pristine site; (C) detailed view of 245 mN (25 gf) Vickers indent and crack system inside a  $10\times$  Brinell zone.

considerably shorter lengths as compared to reference sites. Next to the overlaid Brinell zone Figure 6 also depicts a direct in-scale comparison of Vickers indents outside (Figure 6B) and inside (Figure 6C) of the Brinell zone. By measuring the crack lengths ( $l$ ) and locating all the root positions for all the Vickers indents and the Brinell contact zone radius  $r_0$ , we obtain Figure 7, which demonstrates a clear shortening of the crack lengths inside (with high dislocation density) and outside (with low dislocation density) the Brinell zone. The crack shortening effect increases with cycle count (hence dislocation density, Figure 2), which suggests dislocation-enhanced toughening.

### 3.3 | Crack tip dislocations

The ECCI image for a crack tip region of a reference sample (Figure 8A) indicates some domain structure change, whereas dislocations are absent. In contrast, inside the  $25\times$  Brinell zone, the domains are too fragmented to be resolved, whereas a lot of dislocations along the slip bands are visible. Note that in both cases, the crack flanks are dislocation free, which may be due to the freshly formed free surfaces that attract and absorb the dislocations.

In order to examine the domain structures near the crack tip regions, we also perform PFM measurements as

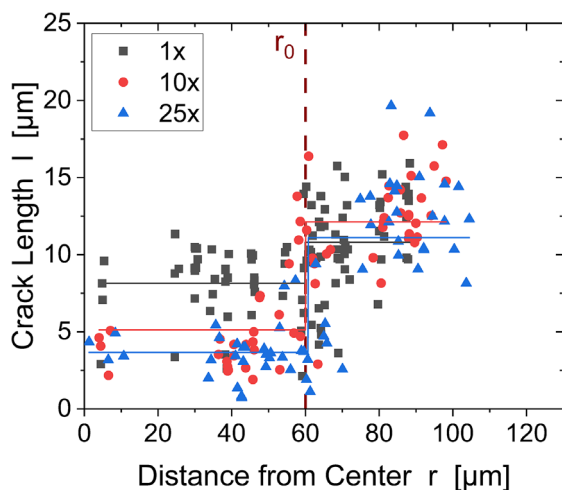


FIGURE 7 Individual crack length as a function of distance from the center of the Brinell indent. The data has been fitted with piecewise constant functions (solid lines in gray, red, and blue) for different numbers of cycles.

depicted in Figure 9. The interaction between the large domain stripes and the crack (Figure 9A) is evident in the reference region, whereas the fragmented domains seem unchanged in the Brinell zone, as they might be immobilized by the dislocation pinning. The white dashed ellipses in Figure 9D suggest nucleation of smaller domains inside a large domain, which may be a possible reason for the domain fragmentation during cyclic loading.

Due to the fact that we were able to pre-engineer dislocations before the crack is induced, we further may quantify the toughening effect induced by dislocations. To this end, we first assess the crack tip toughness using the CTOD method for both cracks in the reference region and inside a 25× Brinell zone. The Irwin parabola (Figure 10) for infinitely long cracks is used as the most basic equation to fit the data and is given by the following equation<sup>27,30,33</sup>:

$$u = \frac{K_{I0}}{E'} \sqrt{\frac{8(a-x)}{\pi}} \quad (1)$$

where  $u$  is half the opening of the crack dependent on the distance from the crack tip,  $a - x$  (see Figure 1, as  $a$  is the crack length and  $x$  is the coordinate along the crack in the propagation direction),  $K_{I0}$  is the crack tip toughness, and  $E'$  is the effective Young's modulus given by  $E/(1 - \nu^2)$ . The fit suggests a 50% increase in crack tip toughness from 0.6 to 0.9 MPa m<sup>0.5</sup>.

In order to evaluate the toughening effect, the ICL method by Casellas et al.<sup>34</sup> for Palmqvist cracks has been applied, as the pre-requirements for the Niihara<sup>32</sup> model for Palmqvist cracks are not fulfilled ( $l/a = 3.2$  for pristine case). The Casellas et al. model is a modified version of the well-established Anstis<sup>35</sup> model, with an adjusted pre-

factor to account for the Palmqvist crack system. Note that the relative increase in the toughening is not influenced by the pre-factor.

For the same cracks used for the CTOD measurement (Figure 10A), fracture toughness values of 0.27 MPa m<sup>0.5</sup> on the reference site and 0.73 MPa m<sup>0.5</sup> inside the 25× Brinell zone were obtained for the ICL method. It is noteworthy that the fracture toughness values from the ICL method differ from the CTOD method, as both methods measure slightly different properties. Regardless of the difference in the absolute fracture toughness values, a consistent toughening effect is observed, with an increase by a factor of 2.8 in the ICL method. The increase in fracture toughness scales in accordance with the enhancement of dislocation density (see Figure S3 in the supplementary materials).

### 3.4 | High-temperature indentation

The Vickers indentation array and the position of the 10× Brinell zone for high-temperature tests (above Curie temperature) are illustrated in Figure 11A. The spatial misplacement of some of the Vickers indents stems from the limited viewing angle with respect to the sample top surface during the in situ testing inside the SEM chamber.

For each indentation array, a clear crack shortening of ~30% (Figure 11B) is observed when comparing the indents inside to outside of the Brinell zone. The presence of crack shortening above the Curie temperature excludes ferroelastic toughening caused by the domain structures observed at room temperature, therefore ascertaining the dislocation-based toughening. In addition, the high-temperature tests also minimize and/or eliminate the potential effect of residual compressive stresses on the crack shortening, which might arise during the previous Brinell indentation performed at room temperature.

We also note that although the sample was later cooled with a minimum cooling rate of 1°C/min and the edges were chamfered, some large cracks, originating from the Vickers indentation-induced cracks, still appeared upon cooling. The cracks induced at high temperatures might be subject to subcritical crack growth during the sample cooling procedure. Therefore, a quantitative measurement of fracture toughness is not feasible at the moment.

## 4 | DISCUSSION

Combining Figures 2 and 6, it suggests that the toughening effect (evidenced by the crack shortening) scales with the pre-engineered dislocation density, with a higher dislocation density resulting in shorter cracks. In parallel,

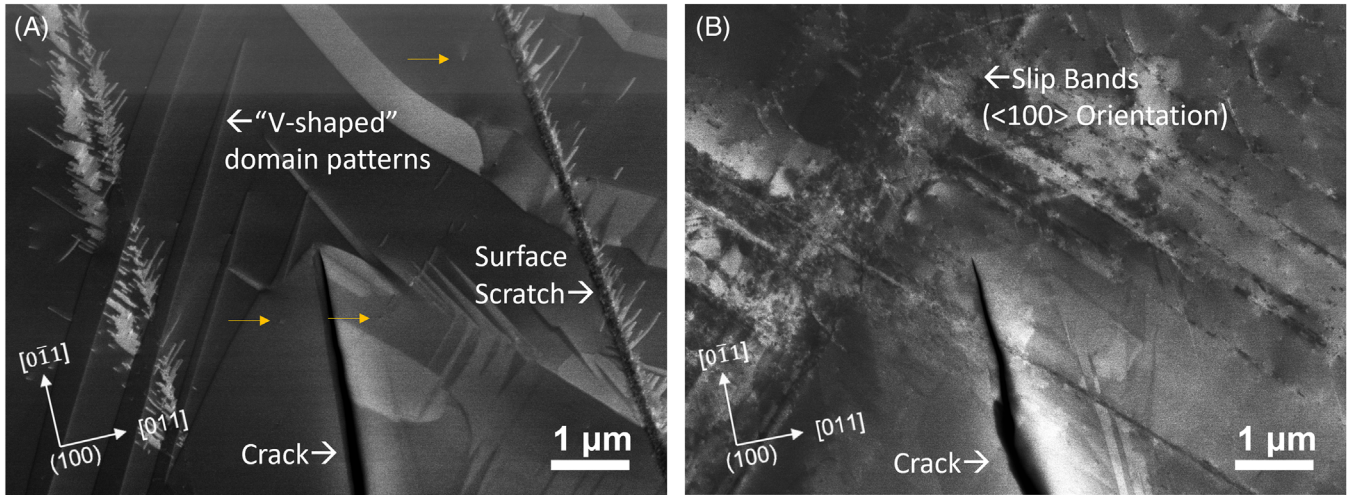


**FIGURE 8** Electron channeling contrast imaging (ECCI) images of (A) crack tip in a reference region, and (B) crack tip inside a 25-cycle Brinell zone.

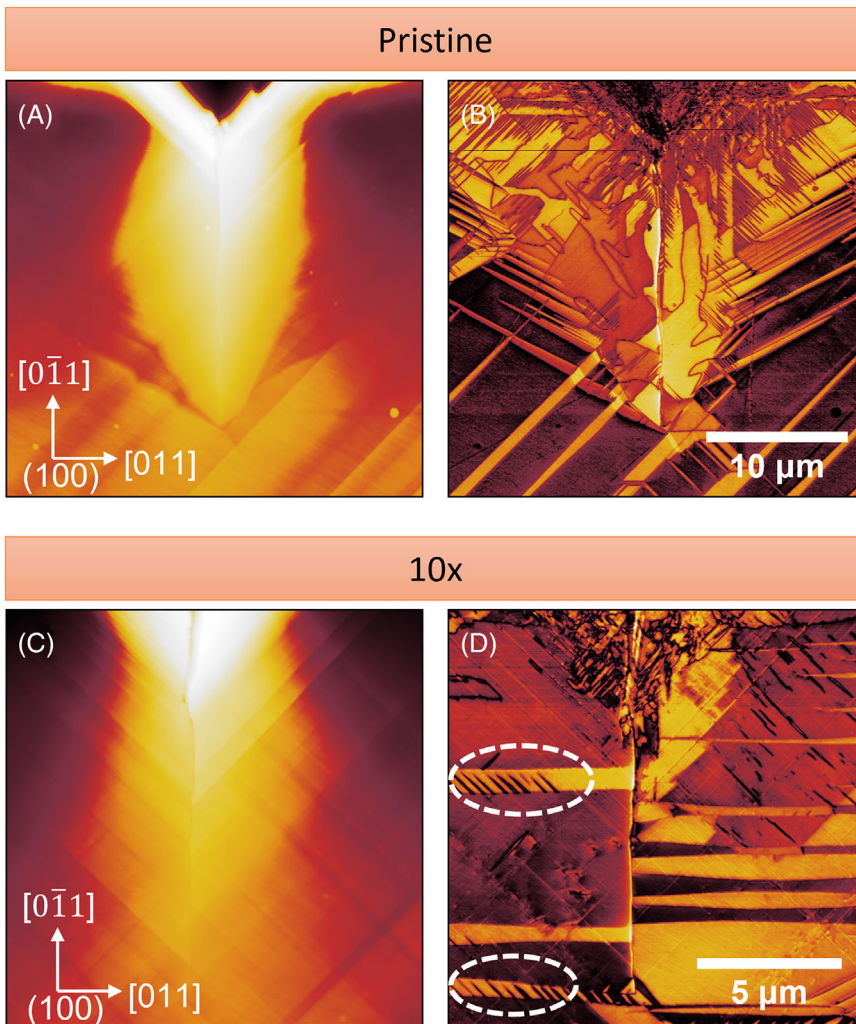


**FIGURE 9** Comparison of piezo-response force microscopy (PFM) images of a crack on a reference region and inside a Brinell zone (with 10 cycles indentation). The vertical crack's "Root" is at the top of the image, the "Tip" at the bottom. Note that the scaling is different for both cases to accommodate the crack shortening effect. (A and C) topography; (B and D) phase amplitude.



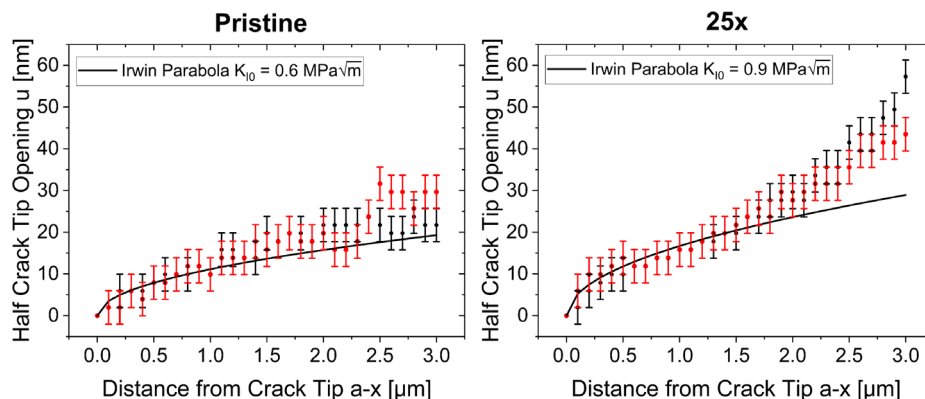


**FIGURE 10** Crack tip opening displacement (CTOD) data for two representative cracks on pristine site and inside 25× Brinell zone with Irwin parabola fit. Error bars represent resolution of scanning electron microscopy (SEM) image as the limiting factor.

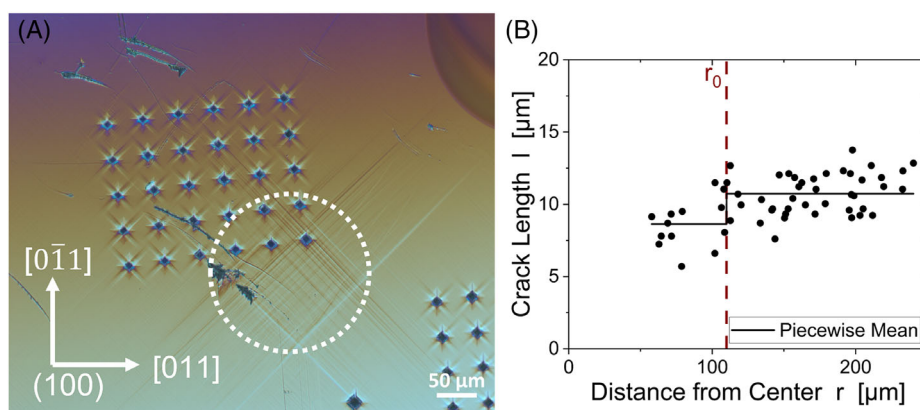


**FIGURE 11** (A) Circumferential interference contrast image of Vickers indent array and the 10× Brinell zone (white dashed line). (B) Vickers indentation crack lengths for the array of indents, fitted with the average values inside and outside of the estimated Brinell zone size.

the domain size is decreased with increasing dislocation density (Figure 4). As ferroelastic toughening is enhanced with large domains, this effect of decreased domain size in the case of cyclically indented regions would rather reduce ferroelastic toughening in contrast to the reference  $\text{KNbO}_3$ .<sup>36–38</sup>

To further completely exclude the ferroelastic toughening by domain structures, we performed high-temperature tests above the Curie temperature. The results in Figure 10 clearly ascertain our assumption that dislocation-based toughening is dominating, although the toughening (crack shortening) is not as pronounced as at room temperature because of the necessary adjustment of experimental parameters (different tips, different loading conditions). A more straightforward method such as micropillar splitting or microcantilever bending<sup>39</sup> will be adopted in the future to focus on the local dislocation-crack tip interactions to better assess the fracture toughness.

Another concern would be the effect of residual (compressive) stresses resulting from the cyclic loading during the Brinell indentation process at room temperature. It

is well known that residual compressive stresses act as closure stresses to suppress crack propagation, which could have a major impact on the crack shortening. To exclude the residual stress, we resort again to the high-temperature indentation tests, which prove a retained dislocation toughening effect.

It is worth mentioning that an annealing step in a conventional oven prior to the Vickers indentation experiments, as in the case of  $\text{SrTiO}_3$  by Salem et al.,<sup>20</sup> turned out to be very challenging due to both the low thermal conductivity of  $\text{KNbO}_3$  and the phase transitions leading to strain incompatibility in the sample. Under controlled heating and cooling rates of  $1\text{--}2^\circ\text{C min}^{-1}$ , the temperature profile during the high-temperature indentation resembles a typical annealing step. Therefore, the residual stress is expected to be minimized in this experiment. A detailed and systematic quantification of the residual stress will be undertaken via HR-EBSD,<sup>40</sup>  $\mu$ -Raman spectroscopy,<sup>41</sup> or FIB cut methods<sup>42</sup> in the future.

In contrast to the similar experiments carried out on  $\text{SrTiO}_3$ ,<sup>20</sup> another oxide perovskite which features

room-temperature plasticity but is paraelectric, the toughening effect in  $\text{KNbO}_3$  turns out to be much more evident (for  $\text{SrTiO}_3$  only  $\sim 20\%$  increase was observed with a dislocation density of  $\sim 10^{14} \text{ m}^{-2}$ ). However, on the other hand,  $\text{SrTiO}_3$  features a much higher resistance to thermal shock as compared to  $\text{KNbO}_3$ . The reason might lie in the phase transitions (tetragonal to cubic and vice versa) during heating/cooling in  $\text{KNbO}_3$ , which are absent for  $\text{SrTiO}_3$ . Another interesting observation is that  $\text{SrTiO}_3$  is known to form broad slip bands ( $1\text{--}50 \mu\text{m}$  in width<sup>43</sup>), whereas  $\text{KNbO}_3$  forms much narrower slip bands or none at all (Figure 3B). Within such broad slip bands, the dislocation motion is limited to the widening of the entire slip band via dislocation multiplication, thereby not contributing to a general enhancement of dislocation toughening. On the other hand, with individual, mobile dislocations in  $\text{KNbO}_3$ , efficient dislocation toughening may occur more readily, yielding a higher toughening effect.

## 5 | CONCLUSION

A high dislocation density (up to  $4 \times 10^{13} \text{ m}^{-2}$ ) was introduced in an area spanning over  $100 \mu\text{m}$  in diameter in single-crystal  $\text{KNbO}_3$  via cyclic Brinell indentation technique at room temperature without forming cracks. By placing Vickers indents inside such large plastic zones, a strong reduction in crack length with increasing dislocation density was attested. Our results suggest a promising approach of using dislocations to enhance fracture toughness in plastically deformable ceramic materials.


- The dislocation density could be enhanced by two orders of magnitude (from  $2 \times 10^{11}$  up to  $4 \times 10^{13} \text{ m}^{-2}$ ) by applying cyclic Brinell indentation up to 25 cycles.
- Maximum effects on crack tip toughness by a factor of 1.5 and of the total fracture toughness by a factor of 2.8 have been achieved.
- High-temperature indentation above the Curie temperature rules out the potential contribution from domains due to ferroelastic toughening and validates the hypothesis that dislocation toughening is the major contributor to this effect.

## ACKNOWLEDGMENTS

The financial support by DFG (No. 414179371) is gratefully acknowledged. X. F. also thanks for the financial support by the Athene Young Investigator program at TU Darmstadt. We thank Dr. Sebastian Bruns for the helpful discussions and Prof. Karsten Durst at TU Darmstadt for access to the laser microscope and SEM.

Open access funding enabled and organized by Projekt DEAL.

## ORCID

Fangping Zhuo  <https://orcid.org/0000-0001-5194-320X>  
Xufei Fang  <https://orcid.org/0000-0002-3887-0111>

## REFERENCES

1. Kingery WD, Bowen HK, Uhlmann DR. Introduction to ceramics. 2nd ed. New York: Wiley; 1976.
2. Ritchie RO. The conflicts between strength and toughness. *Nat Mater*. 2011;10(11):817–22.
3. Niu H, Niu S, Oganov AR. Simple and accurate model of fracture toughness of solids. *J Appl Phys*. 2019;125(6):65105.
4. Gilman JJ, Johnston WG. Dislocations in lithium fluoride crystals. *Solid State Phys*. 1962;13:147–222.
5. Johnston WG, Gilman JJ. Dislocation multiplication in lithium fluoride crystals. *J Appl Phys*. 1960;31(4):632–43.
6. Johnston WG, Gilman JJ. Dislocation velocities, dislocation densities, and plastic flow in lithium fluoride crystals. *J Appl Phys*. 1959;30(2):129–44.
7. Gilman JJ. Nucleation of dislocation loops by cracks in crystals. *JOM*. 1957;9(4):449–54.
8. Gilman JJ, Johnston WG. Observations of dislocation glide and climb in lithium fluoride crystals. *J Appl Phys*. 1956;27(9):1018–22.
9. Porz L. 60 years of dislocations in ceramics: a conceptual framework for dislocation mechanics in ceramics. *Int J Ceram Eng Sci*. 2022;4(4):214–39.
10. Hameed S, Pelc D, Anderson ZW, Klein A, Spieker RJ, Yue L, et al. Enhanced superconductivity and ferroelectric quantum criticality in plastically deformed strontium titanate. *Nat Mater*. 2022;21(1):54–61.
11. Muhammad QK, Porz L, Nakamura A, Matsunaga K, Rohnke M, Janek J, et al. Donor and acceptor-like self-doping by mechanically induced dislocations in bulk  $\text{TiO}_2$ . *Nano Energy*. 2021;85:105944.
12. Höfling M, Zhou X, Riemer LM, Bruder E, Liu B, Zhou L, et al. Control of polarization in bulk ferroelectrics by mechanical dislocation imprint. *Science*. 2021;372(6545):961–4.
13. Messerschmidt U. Dislocation dynamics during plastic deformation. 1st ed. Berlin, Heidelberg, Cham: Springer Berlin Heidelberg; Springer International Publishing AG; 2010.
14. Appel F, Messerschmidt U, Kuna M. Crack propagation in MgO during in-situ deformation in the high-voltage electron microscope. *Phys Status Solidi (a)*. 1979;55(2):529–36.
15. Narita N, Higashida K, Kitano S. Dislocation distribution around a crack tip and the fracture toughness in NaCl crystals. *Scr Metall*. 1987;21(10):1273–8.
16. Narita N, Higashida K, Torii T, Miyaki S. Crack-tip shielding by dislocations and fracture toughness in NaCl crystals. *Mater Trans JIM*. 1989;30(11):895–907.
17. Moon W-J, Saka H. Toughening of a brittle material by means of dislocation subboundaries. *Philos Mag Lett*. 2000;80(7):461–6.
18. Porz L, Klomp AJ, Fang X, Li N, Yildirim C, Detlefs C, et al. Dislocation-toughened ceramics. *Mater Horiz*. 2021;8(5):1528–37.
19. Issa I, Gammer C, Kolitsch S, Hohenwarter A, Imrich PJ, Pippan R, et al. In-situ TEM investigation of toughening in silicon at small scales. *Mater Today*. 2021;48:29–37.
20. Salem MN, Ding K, Rödel J, Fang X. Thermally enhanced dislocation density improves both hardness and fracture toughness

- in single-crystal SrTiO<sub>3</sub>. *J Am Ceram Soc.* 2022;106:1344–35. <https://doi.org/10.1111/jace.18839>
21. Taylor GI. Plastic strain in metals. *J Inst Met.* 1938;62:307–24.
  22. Okafor C, Ding K, Zhou X, Durst K, Rödel J, Fang X. Mechanical tailoring of dislocation densities in SrTiO<sub>3</sub> at room temperature. *J Am Ceram Soc.* 2021;105:2399–402. <https://doi.org/10.1111/jace.18277>
  23. Höfling M, Trapp M, Porz L, Uršič H, Bruder E, Kleebe H-J, et al. Large plastic deformability of bulk ferroelectric KNbO<sub>3</sub> single crystals. *J Eur Ceram Soc.* 2021;41(7):4098–107.
  24. Mark AF, Castillo-Rodriguez M, Sigle W. Unexpected plasticity of potassium niobate during compression between room temperature and 900°C. *J Eur Ceram Soc.* 2016;36(11):2781–93.
  25. Hirel P, Mark AF, Castillo-Rodriguez M, Sigle W, Mrovec M, Elsässer C. Theoretical and experimental study of the core structure and mobility of dislocations and their influence on the ferroelectric polarization in perovskite KNbO<sub>3</sub>. *Phys Rev B.* 2015;92(21):214101.
  26. Zaefferer S, Elhami N-N. Theory and application of electron channelling contrast imaging under controlled diffraction conditions. *Acta Mater.* 2014;75:20–50.
  27. Fett T, Kounga Njiwa AB, Rödel J. Crack opening displacements of Vickers indentation cracks. *Eng Fract Mech.* 2005;72(5):647–59.
  28. Seidel J, Rödel JS. Measurement of crack tip toughness in alumina as a function of grain size. *J Am Ceram Soc.* 1997;80(2):433–8.
  29. Haubensak F, Argon AS. A new method of fracture toughness determination in brittle ceramics by open-crack shape analysis. *J Mater Sci.* 1997;32(6):1473–7.
  30. Irwin GR. Analysis of stresses and strains near the end of a crack traversing a plate. *J Appl Mech.* 1957;24(3):361–4.
  31. Quinn GD. Fracture toughness of ceramics by the vickers indentation crack length method: a critical review. *Ceram Eng Sci Proc.* 2006;27(3):45–62.
  32. Niihara K, Morena R, Hasselman DPH. Evaluation of K<sub>Ic</sub> of brittle solids by the indentation method with low crack-to-indent ratios. *J Mater Sci Lett.* 1982;1(1):13–6.
  33. Vögler M, Fett T, Rödel J. Crack-tip toughness of lead-free (1-x)(Na<sub>1/2</sub>Bi<sub>1/2</sub>)TiO<sub>3</sub> - xBaTiO<sub>3</sub> piezoceramics. *J Am Ceram Soc.* 2018;101(12):5304–8.
  34. Casellas D, Nagl MM, Llanes L, Anglada M. Microstructural coarsening of zirconia-toughened alumina composites. *J Am Ceram Soc.* 2005;88(7):1958–63.
  35. Anstis GR, Chantikul P, Lawn BR, Marshall DB. A critical evaluation of indentation techniques for measuring fracture toughness: I, direct crack measurements. *J Am Ceram Soc.* 1981;64(9):533–8.
  36. Santos e Lucato SL, Lupascu DC, Rödel J. Effect of poling direction on R-curve behavior in lead zirconate titanate. *J Am Ceram Soc.* 2000;83(2):424–6.
  37. Yang W, Zhu T. Switch-toughening of ferroelectrics subjected to electric fields. *J Mech Phys Solids.* 1998;46(2):291–311.
  38. Zhu T, Yang W. Toughness variation of ferroelectrics by polarization switch under non-uniform electric field. *Acta Mater.* 1997;45(11):4695–702.
  39. Ast J, Ghidelli M, Durst K, Göken M, Sebastiani M, Korsunsky AM. A review of experimental approaches to fracture toughness evaluation at the micro-scale. *Mater Des.* 2019;173:107762.
  40. Wilkinson AJ, Meaden G, Dingley DJ. High-resolution elastic strain measurement from electron backscatter diffraction patterns: new levels of sensitivity. *Ultramicroscopy.* 2006;106(4–5):307–13.
  41. Wermelinger T, Spolenak R. Symmetry of residual stress fields of ZnO below an indent measured by three-dimensional Raman spectroscopy. *J Appl Phys.* 2009;106(6):64907.
  42. Korsunsky AM, Sebastiani M, Bemporad E. Residual stress evaluation at the micrometer scale: analysis of thin coatings by FIB milling and digital image correlation. *Surf Coat Technol.* 2010;205(7):2393–403.
  43. Porz L, Frömling T, Nakamura A, Li N, Maruyama R, Matsunaga K, et al. Conceptual framework for dislocation-modified conductivity in oxide ceramics deconvoluting mesoscopic structure, core, and space charge exemplified for SrTiO<sub>3</sub>. *ACS Nano.* 2021;15(6):9355–67.

## SUPPORTING INFORMATION

Additional supporting information can be found online in the Supporting Information section at the end of this article.

**How to cite this article:** Preuß O, Bruder E, Lu W, Zhuo F, Minnert C, Zhang J, et al. Dislocation toughening in single-crystal KNbO<sub>3</sub>. *J Am Ceram Soc.* 2023;106:4371–4381. <https://doi.org/10.1111/jace.19088>